IOP Conf. Series: Materials Science and Engineering **280** (2017) 012005 doi:10.1088/1757-899X/280/1/012005

Numerical Modelling and Analysis of Hydrostatic Thrust Air Bearings for High Loading Capacities and Low Air Consumption

Yunluo Yu, Guang Pu and Kyle Jiang*

University of Birmingham, Birmingham B15 2TT, United Kingdom

*K.Jiang@bham.ac.uk

Abstract. The paper presents a numerical simulation study on hydrostatic thrust air bearings to assess the load capacity, compressed air consumptions, and the dynamic response. Finite Difference Method (FDM) and Finite Volume Method (FVM) are combined to solve the non-linear Reynolds equation to find the pressure distribution of the air bearing gas film and the total loading capacity of the bearing. The influence of design parameters on air film gap characteristics, including the air film thickness, supplied pressure, depth of the groove and external load, are investigated based on the proposed FDM model. The simulation results show that the thrust air bearings with a groove have a higher load capacity and air consumption than without a groove, and the load capacity and air consumption both increase with the depth of the groove. Bearings without the groove are better damped than those with the grooves, and the stability of thrust bearing decreases when the groove depth increases. The stability of the thrust bearings is also affected by their loading.

1. Introduction

Hydrostatic air film thrust bearings are very important machine elements to support lightly loaded, high speed rotating machinery such as spindles, gas expanders, compressors, and micro gas turbines. Previous studies on the design of thrust air bearings mainly focused on static characteristics [1-3]. However, in a high speed rotational system, such as a spindle, pressure fluctuations and bearing air film variations in thrust bearings caused by various factors, such as different loads and rotating speeds, induce excitations of the bearing dynamic response, which can lead to bearing instability. Therefore, developing an effective tool to analysis the dynamic responses as well as the static characteristics of hydrostatic thrust air bearings is of great importance for designing high quality and high speed rotational machinery.

Numerical analysis is the main methodology used in the investigation of the modern thrust air bearings. Developing accurate numerical models for the design of thrust air bearings is one of the major tasks in the field. Fundamentally the work is to solve the Reynolds Equation numerically. Three discrete schemes can be used together with Newton's method to solve the second order partial differential equation: Finite Difference Method (FDM), Finite Element Method (FEM) and the Finite Volume Method (FVM). Florin suggested that by applying Newton's method, it can reduce computational time significantly [4]. Newton's method is also proven to have a good stability in getting converged solutions [5]. Nenzi Wang carried out a series of studies on numerical methods which can be applied to solve a compressible Reynolds Equation [6-8]. The work includes

comparisons of different methods with respect to computational time and stability. He also suggested different stopping criterion in an iterative process and analysed the truncation error of numerical approaches [6-8]. The above mentioned approaches are all based on FDM and they have good agreement with the experiment results of hydrostatic air bearings. FVM is also suggested by some researchers. It is based on the continuity equation and Green's theorem. This approach shows advantages in dealing with film discontinuities and some pocket restrictor configuration [9].

In this paper, a numerical model of hydrostatic thrust air bearings is proposed combining the advantages of FDM and FVM for solving the Reynolds Equation. Then motion equations are added into the model to simulate the dynamic response of the thrust air bearing. Finally, the effect of several design and working parameters on air film characteristics, including the air film thickness, supplied pressure, depth of the groove and external load, are investigated based on the proposed model.

2. Modeling

2.1. Reynolds equations and the finite difference scheme

In this section, a numerical model based on the finite different method and finite volume method is developed for hydro-static air bearings in order to study the effect of several design parameters on air film gap characteristics, including the air film thickness, supplied pressure, depth of the groove and external load.

After introducing the dimensionless variables:

$$R = \frac{r}{r_2}, P = \frac{p}{p_a}, H = \frac{h}{h_0}, u = \frac{\omega r_2}{2}, \tau = \omega t$$

where r_2 is the outer radius of the bearing, p_a the atmospheric pressure, h_0 the reference film thickness, h the film thickness, t time. With the isentropic gas, the Reynolds equation of compressible flow can be written as Eq.(1):

$$\frac{\partial}{\partial R}\left(RPH^3\frac{\partial P}{\partial R}\right) + \frac{1}{R}\frac{\partial}{\partial \theta}\left(PH^3\frac{\partial P}{\partial \theta}\right) = \Lambda R\frac{\partial (PH)}{\partial \theta} + 2\Lambda R\frac{\partial (PH)}{\partial \tau} \tag{1}$$

$$\Lambda = \frac{6\mu\omega r_2}{p_a h_0{}^2} \tag{2}$$

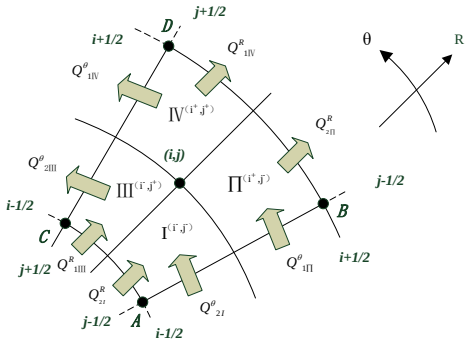

Figure 1. The defined control volume

where Λ is the compressibility number or bearing number and μ the viscosity of air. To solve the Reynolds Equation, a control volume is defined in Fig.1, and the mass flow rate Q^R across the boundary of $R = constant$ and the mass flow rate Q^θ across the boundary of $\theta = constant$ are calculated respectively as follows:

$$Q^R = \int_{R_1}^{R_2}(-RPH^3\frac{\partial P}{\partial R} + \Lambda RPH)dR \tag{3}$$

$$Q^\theta = \int_{\theta_1}^{\theta_2}(-PH^3\frac{\partial P}{\partial \theta})d\theta \tag{4}$$

The mass flow rate due to squeezing motion inside the control volume is expressed as follows:

$$Q^{\tau} = \int_{\theta_1}^{\theta_2} \int_{R_1}^{R_2} (2\Lambda R \frac{\partial PH}{\partial \tau}) dR d\theta \tag{5}$$

The following relationship can be found from the mass flow rate balance on the control volume:

$$Q^{\theta}{}_{2I} + Q^{\theta}{}_{1III} - Q^{\theta}{}_{2II} - Q^{\theta}{}_{1IV} + Q^{R}{}_{2I} + Q^{R}{}_{1II} - Q^{R}{}_{2III} - Q^{R}{}_{1IV} = Q^{\tau} + Q^{orifice} \tag{6}$$

where $Q^{orifice}$ is the mass flow rate of the orifice. The dimensionless mass flow rate of the orifice can be calculated according to the following equations under isentropic assumption:

$$Q^{orifice} = \begin{cases} HC_s \left\{ \frac{2}{\gamma - 1} \left[\left(\frac{P_r}{P_s} \right)^{2/\gamma} - \left(\frac{P_r}{P_s} \right)^{(\gamma+1)/\gamma} \right] \right\}^{1/2}, & if \ \frac{P_r}{P_s} \geq \left(\frac{2}{\gamma+1} \right)^{(\gamma-1)/\gamma} \\ HC_s \left(\frac{2}{\gamma+1} \right)^{\left(\frac{(\gamma+1)}{2(\gamma-1)} \right)}, & if \ \frac{P_r}{P_s} < \left(\frac{2}{\gamma+1} \right)^{(\gamma-1)/\gamma} \end{cases} \tag{7}$$

$$C_s = \frac{12\mu\pi d C_d P_s}{h_0^2 p_{at}^2} \sqrt{\gamma \Re T} \tag{8}$$

where T is the atmospheric temperature at supply conditions, C_d the discharge coefficient, d the orifice diameter, μ the dynamic viscosity of the fluid, γ the isentropic index and $\Re$ the gas constant. Powel [10] regarded C_d as a function of the pressure ratio $\frac{P_r}{P_s}$. However, many researchers take the coefficient as 0.8 for all flow conditions [11]. In this study, C_d is taken as 0.8 in all the cases. By solving Eq.(1), the pressure distribution of the lubricating can be found.

2.2. Calculation of static characteristics

For a thrust bearing experiencing a small vibration in the axial direction, the minimum air film thickness and pressure can be expressed as:

$$h = h_0 + \varepsilon e^{j\omega_f t}$$
$$p = p_0 + \varepsilon p_t e^{j\omega_f t} \tag{9}$$

where ε represents the function of air film thickness and the bound of ε is approximately within ±10 percent of the steady state air film thickness. Subscripts 0 and t mean the physical quantities under the steady and unsteady operation conditions, respectively.

Based on the equilibrium on the control volume, the following relationships can be obtained:

$$F_0(P_0) = Q^{\theta}{}_{2I0} + Q^{\theta}{}_{1III0} - Q^{\theta}{}_{2II0} - Q^{\theta}{}_{1IV0} + Q^{R}{}_{2I0} + Q^{R}{}_{1II0} - Q^{R}{}_{2III0} - Q^{R}{}_{1IV0} - Q^{orifice} = 0 \tag{10}$$

$$F_t(P_t, P_0) = Q^{\theta}{}_{2Is} + Q^{\theta}{}_{1IIIs} - Q^{\theta}{}_{2IIs} - Q^{\theta}{}_{1IVs} + Q^{R}{}_{2Is} + Q^{R}{}_{1IIs} - Q^{R}{}_{2IIIs} - Q^{R}{}_{1IVs} - Q^{\tau}{}_{s} - Q^{orifice} = 0 \tag{11}$$

Eq. (10) is a nonlinear equation which can be solved by applying the Newton-Raphson iteration algorithm. Eq.(11) is a linear equation which can be solved based on the steady state pressure P_0 obtained through Eq.(10).

In this work, maximization of the bearing load capacity and minimization of the consumption of compressed air are considered as the way to the optimal design of the hydrostatic thrust bearings. The consumption of compressed air is the air flow rate of all the orifice restrictors. The load capacity can be calculated using Eq. (12):

$$w = \int_{r_1}^{r_2} \int_{0}^{2\pi} (p_0 - p_a) r dr d\theta \tag{12}$$

2.3. Calculation of dynamic responses

The calculation requires to solve the Reynolds equation with the equation of motion [12-13] simultaneously. The Reynolds equations have been introduced in Section 2.2. The equation of motion can be written as:

$$\Delta w(t) = m\ddot{h} \tag{13}$$

where m is the mass supported by the bearing, Δw is the variation of the resultant pressure force. The dynamic response of thrust air bearing can be calculated using the following scheme:

1. Choose an equilibrium position of the simulated thrust bearing for dynamic calculation.
2. Input initial step displacements and velocities for step by step method.
3. Dynamic calculation of the movement (acceleration, velocity, displacement, pressure and load capacity, etc.)

3. Numerical simulation

3.1. Thrust bearings for simulation

In this section, 4 types of hydrostatic thrust air bearings, as shown in Fig. 2 and Tab.1, are simulated using the FDM and FVM. The influences of several design parameters on air film characteristics, including the air film thickness, the pressure of supplied air, the depth of the groove, and the external loading, are investigated to provide information in the future design of hydrostatic thrust air bearing.

Table 1. Description of bearings simulated

Geometric parameters	Thrust bearing without a groove	Thrust bearings with a groove		
	Type 1	Type 2	Type 3	Type 4
r_2(mm)	15	15	15	15
r_1(mm)	6	6	6	6
h_g(um)	-	10	20	30

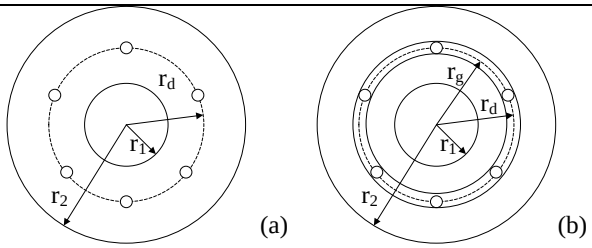

Figure 2. (a) Hydrostatic thrust air bearing without grooves and (b) Hydrostatic thrust air bearing with a groove.

Other fixed parameters are listed in Table 2.

Table 2 Fixed parameters of bearings studied

Bearing parameters	Value	Bearing parameters	Value
Reference gap h_0(um)	20	Coefficient of discharge C_d	0.8
Radius of orifices r_d	10.5×10^{-3}	Isentropic index γ	1.4
Radius of the groove r_g	10.5×10^{-3}	Gas constant $\mathcal{R}$ (J kg^{-1} K^{-1})	287
Diameter of orifices d_0	250×10^{-6}	Dynamic viscosity u (Pa s)	18.38×10^{-6}
Supply pressure p_s (Pa)	6×10^{-5}	Temperature at supply conditions T (^{o}K)	293

3.2. Analysis of static characteristics

If air consumption needs to be reduced as much as possible while maintaining a reasonable load capacity, the influence of air film thickness, supplied pressure, depth of the groove and the effect of supplied pressure on load capacity and mass flow rate can be investigated.

The load capacity and mass flow rate of all the orifice restrictors calculated versus the air film thickness are respectively presented in Figs.3 and 4. The results are for $p_s = 3 \times 10^5$ Pa, $n_{ori} = 6$ and $\omega = 0$ rpm. From Figs.3 and 4, it can be seen that the load capacity is inversely proportional to the air film thickness while the mass flow rate is proportional to the air film thickness, which means a lower air film thickness can lead to a higher load capacity and lower compressed air consumption. In comparison of the load capacity and the mass flow rate of the 4 thrust air bearings, it can be seen that the bearings with groove, namely Type 2, Type 3 and Type 4, have a higher load capacity but larger air consumption than those without grooves. In addition, a deeper groove leads to a higher load capacity and larger air consumption, such as Type 4.

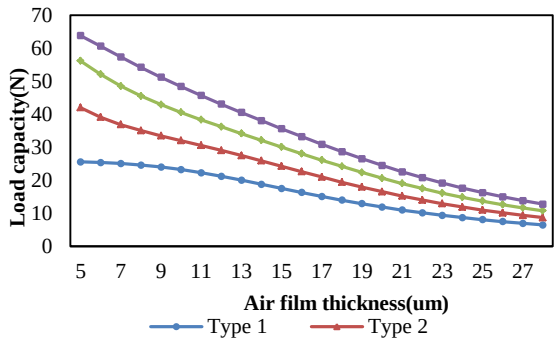

Figure 3. Static load capacity versus air film thickness for the 4 types of thrust bearings

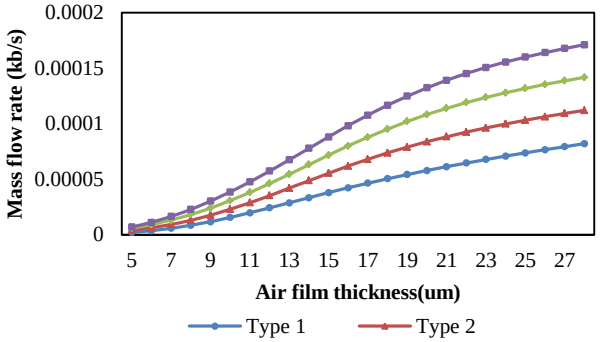

Figure 4. Mass flow rate versus air film thickness for the 4 types of thrust bearings

The load capacity and mass flow rate of all the orifice restrictors calculated versus the supplied pressure are respectively presented in Fig.5 and Fig.6. Results are obtained for $h_0 = 20 \times 10^6$ um, $n_{ori} = 6$ and $\omega = 0$ rpm.

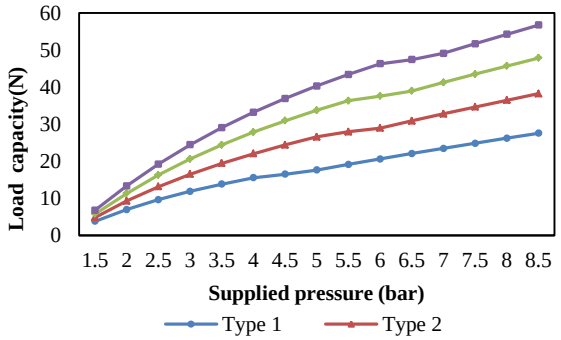

Figure 5. Static load capacity versus supplied pressure for the 4 thrust bearings

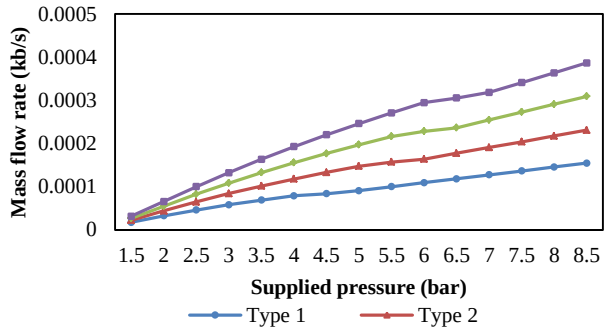

Figure 6. Mass flow rate versus supplied pressure for the 4 thrust bearings

Figs.5 and 6 show that the load capacity and the mass flow rate are both proportional to supplied pressure for the 4 bearings. Comparing their load capacities and the mass flow rates, it can be seen that the bearings 2, 3 and 4 with a groove achieve a higher load capacity and mass flow rate than the bearing without a groove, i.e. bearing 1. Once again, it proves that the deeper the grooves are, the higher the load capacity and air consumption.

3.3. Analysis of dynamic response

Figs.7 and 8 depict the dynamic step responses of the 4 thrust bearings. The step responses are calculated with the scheme described in Section 2.3. The same initial conditions used in all the cases are $h_0 = 20\mu m, \dot{h_o} = 0, P_s = 6\ bar, \omega = 10000 rpm,$ and $dt = 10^{-5} s$. The dynamic simulation took 2 external loadings into consideration: $w_1 = 5N$ and $w_2 = 20N$.

With an external load of 5N, the step responses of the bearings are undamped for Type 2, Type 3 and Type 4; however, the step response of Type 1 bearing is damped, which means thrust bearings without a groove have a better stability compared with those with a groove. The same conclusion can be found in Reference [14], which tested the nature frequency of the thrust bearings with and without a groove experimentally, and proved that the bearings without a groove is better damped than the bearing with a groove. Nevertheless, it can be concluded from Fig 8 that the stability decreases when the groove depth increases.

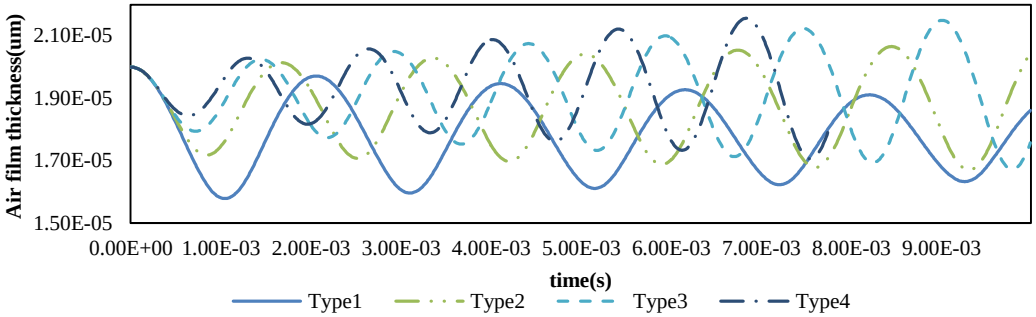

Figure 7. The dynamic step responses of the 4 types thrust air bearings for $w_1 = 5N$.

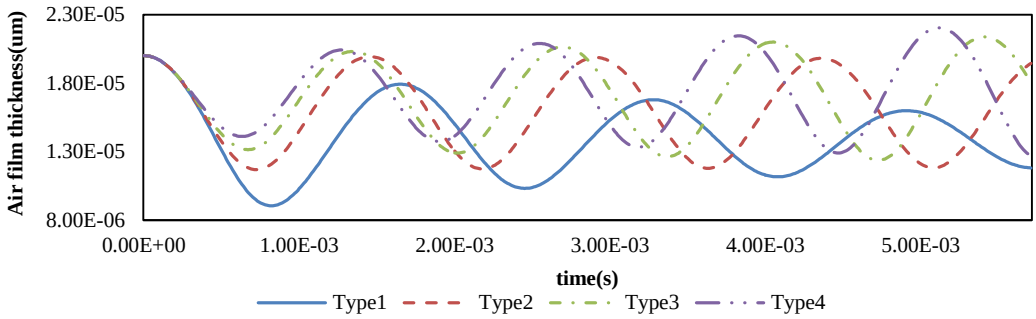

Figure 8. The dynamic step responses of the 4 types thrust air bearings for $w_2 = 20N$

With an external loading of 20N, the dynamic step responses of Types 3 and 4 are still not damped, but damped for Type 1 and Type 2 thrust bearings, and the Type 1 thrust bearing still performs the best stability. It needs to be noticed that for the external load $w_1 = 5N$, Type 2 cannot get a damped response; but for the external load $w_2 = 20N$, the dynamic response for Type 2 thrust bearing got damped. This means the stability of thrust bearing can be greatly affected by the external load. Same conclusion can be found in Reference [14].

4. Conclusions

In this paper, a numerical model of thrust air bearings, based on FDM and FVM, is presented. The load capacity, compressed air consumptions, and the dynamic response of hydro-static thrust air bearings are investigated based on the proposed model. The numerical results show that the thrust bearings with a circular groove can always get a higher load capacity and higher air consumption than the thrust bearing without the groove, and the load capacity and the air consumption is proportional to the groove depth. The bearing without the groove is better damped than the bearings with the groove, which means the stability of thrust bearing decreases when the groove depth increases. In addition, hydrostatic thrust bearings with a circular groove would lose the stability with a high external load. These findings can be taken into consideration in the design of a thrust air bearing.

Acknowledgments

The research is supported, in part, by European Horizon 2020 project 644971, Department for Transport T-TRIG 2017 project, and the scholarship from China Scholarship Council (CSC).

References

[1] Lipschitz A, Basu P, Johnson R P. A bi-directional gas thrust bearing[J]. Tribology transactions, 1991, 34(1): 9-16.
[2] Huitric J, Tournerie B. Finite element analysis of grooved gas thrust bearings and grooved gas face seals[J]. Journal of tribology, 1993, 115: 349.
[3] Artiles A, Shapiro W, Jones H F. Design analysis of Rayleigh-step floating-ring seals[J]. ASLE transactions, 1984, 27(4): 321-331.
[4]Radu F A, Pop I S, Knabner P. Newton—Type Methods for the Mixed Finite Element Discretization of Some Degenerate Parabolic Equations[M]. Numerical mathematics and advanced applications. Springer Berlin Heidelberg, 2006: 1192-1200.
[5] Waumans T, Peirs J, Reynaerts D, et al. On the dynamic of high-speed gas bearings: stability study and experimental validation[C]. Proceedings of the 3rd Conference on Sustainable Construction and Design. 2011: 342-351.
[6] Wang N, Chang C. An application of Newton's method to the lubrication analysis of air-lubricated bearings[J]. Tribology transactions, 1999, 42(2): 419-424.
[7] Wang N, Chang S H, Huang H C. Comparison of Iterative Methods for the Solution of Compressible-Fluid Reynolds Equation[J]. Journal of Tribology, 2011, 133(2): 021702.
[8] Wang N, Chang S H, Huang H C. Stopping Criterion in Iterative Solution Methods for Reynolds Equations[J]. Tribology Transactions, 2010, 53(5): 739-747.
[9] Arghir M, Alsayed A, Nicolas D. The finite volume solution of the Reynolds equation of lubrication with film discontinuities[J]. International Journal of Mechanical Sciences, 2002, 44(10): 2119-2132.
[10] Powell J W. Design of aerostatic bearings[J]. The Machinery Published Co. Ltd.1970.
[11] Neves MT, Schwarz VA, Menon GJ. Discharge coefficient influence on the performance of aerostatic journal bearings. Tribol Int 2010;43:746–51.
[12] Charki A, Bigaud D, Guérin F. Behavior analysis of machines and system air hemispherical spindles using finite element modeling. Ind Lubr Tribol 2013;65(4).
[13] Bonis M, Charki A. Modélisation des caractéristiques statiques et de la stabilité des paliers de butée aérostatiques par la méthode des éléments Finis[J]. Revue Européenne des Eléments, 2001, 10(6-7): 755-767.
[14] Charki A, Diop K, Champmartin S, et al. Numerical simulation and experimental study of thrust air bearings with multiple orifices[J]. International Journal of Mechanical Sciences, 2013, 72: 28-38.